

Accurate Inductance De-embedding Technique for Scalable Inductor Models

Volker Blaschke and James Victory
Jazz Semiconductor
4321 Jamboree Rd

Newport Beach, CA 92660
volker.blaschke@jazzsemi.com

Abstract - Scalable models for circuit design components such as inductors are a requirement for state of the art design environments. Accurate Spice-level modeling requires physical based models and an accurate RF characterization process. In this paper we present a semi-analytical de-embedding technique that accounts for the magnetic coupling between test structure feed-lines and device under test (DUT). The method significantly improves the result of extracted inductance and enables broadband frequency characterization of square and octagonal inductors in single-ended and differential configuration over a large space of geometries.

Index Terms – Inductors, test-structure, RF-measurement, de-embedding, magnetic coupling, inductance accuracy.

I. INTRODUCTION

Integrated inductors are a key component to modern day RF design where they are heavily used in tuning, filtering and impedance matching applications. An efficient and reliable RF design process requires scalable broadband Spice-level models of single-ended and differential inductors, seamlessly integrated into process design kits (PDK) [1]. The model accuracy has to be validated with RF-measurements covering a large geometry range, including sub nH inductors which are very susceptible to de-embedding errors.

A microscope picture of a single-ended and a differential inductor embedded in 2-port ground-signal-ground pads for RF measurement is shown in Fig.1 and Fig.2. The test structure adds considerable parasitic R, L and C that have to be de-embedded from the measurements to yield the intrinsic device. Conventional 2 step, 3 step and 4 step de-embedding techniques [2]-[8] using open, short and thru test structures do not capture the magnetic coupling between signal feed-lines and the DUT. In some cases for 1 turn inductors,

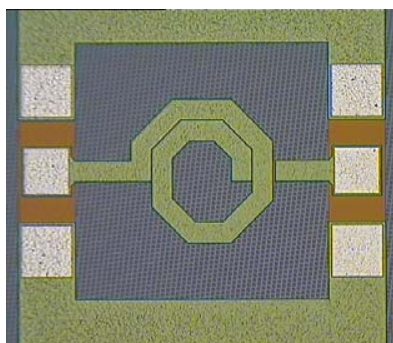


Fig.1. Single-ended octagonal inductor in 2-port ground-signal-ground pad configuration.

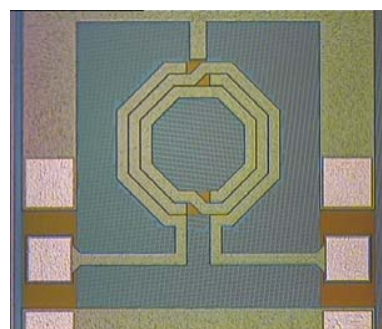


Fig.2. Differential octagonal inductor in 2-port ground-signal-ground pad configuration with center tab grounded through test fixture ground return frame.

the inductance of the feed-line can be on the same order as the DUT, and the mutual inductance due to magnetic coupling is substantial. Alternative routing of the feed-lines may help reduce the mutual coupling, but generally not to a negligible level if accurate results are desired.

In section II, we explain the importance of the magnetic coupling effect between test structure and the intrinsic device to be characterized. A new method that accurately computes the magnetic coupling and accounts for it in the de-embedding process is described in section III. Finally measurements and electromagnetic simulation results are shown in section IV to validate the de-embedding process.

II. EFFECT OF FEED LINE MUTUAL INDUCTANCE

The picture in Fig.3 indicates the flow of the current in an octagonal 1.5 turn inductor in single-ended configuration. The current flow in the test structure feed segments generates a positive mutual inductance with the upper half and a

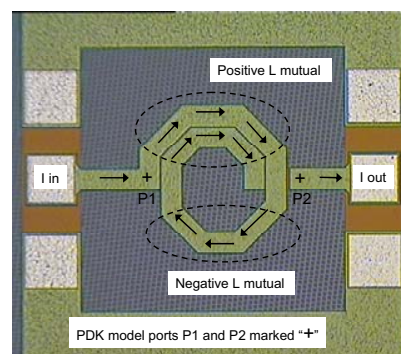


Fig.3. Single-ended octagonal inductor with indication of current flow and mutually coupled segments.

negative mutual inductance with the lower half of the inductor. There is no mutual inductance produced with the vertical segments. This mutual feed coupling effect will result in an overestimate of the inductance of the de-embedded intrinsic device, due to the presence of more positive than negative coupled segments in this particular inductor. The PDK model represents the intrinsic inductor to the port locations marked in the picture and does not account for the mutual coupling effect.

The current flow through the feed-lines and inductor segments determines the sign of the mutual coupling and can introduce large inaccuracies if not properly accounted for. The measurement results of a single-ended square inductor with clockwise (CW) and counter-clockwise (CCW) winding orientation as schematically drawn in Fig.4 and Fig.5 demonstrates that the mutual inductive coupling with the feed lines can be severe.

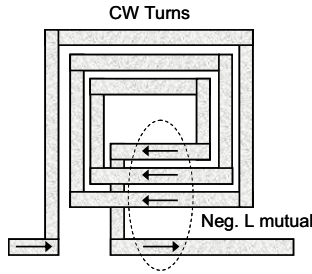


Fig.4. Single-ended 3-turn square inductor with clockwise winding and negative magnetic coupling to signal feed-lines.

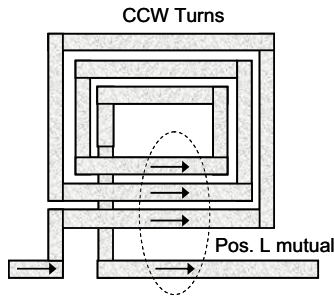


Fig.5. Single-ended 3-turn square inductor with counter-clockwise winding and positive magnetic coupling to signal feed-lines.

The intrinsic device inductance for both cases is identical. For the CW winding, the current flow in single-ended configuration will give rise to a negative mutual inductance with the device, causing the extracted inductance result for conventional de-embedding to be ~ 230 pH lower than the expected device inductance of 2.7 nH, an error close to 9% (Fig.6). With CCW winding, the mutual inductance will be positive and the extracted results higher than the expected inductance. The difference between both winding orientations is on the order of 500 pH. By accounting for this mutual inductance in the de-embedding process, the inductance of the intrinsic device is extracted for both devices as ~ 2.7 nH.

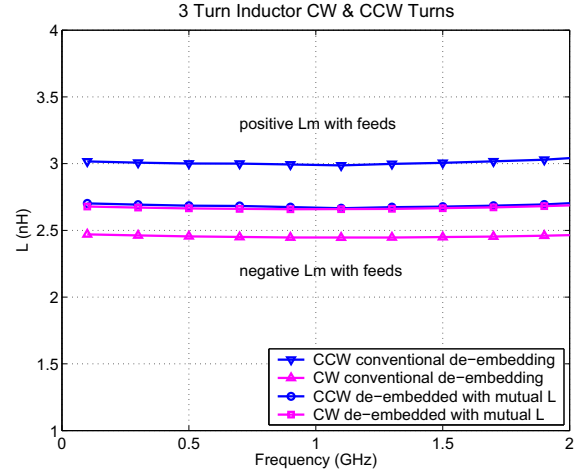


Fig.6. Effect of turn orientation on inductance result.

III. SEMI-ANALYTICAL DE-EMBEDDING PROCESS

A. Calculation of Feed-Line and Mutual Inductance

The new method relies on accurate computation of the feed-line self-inductance and mutual inductance to the DUT. Self-inductance and mutual inductance between parallel segments are calculated using the Greenhouse equations [9]. Mutual inductance with off-angle segments in the octagonal inductors are calculated with Grover's equation [10] for central filaments at an angle:

$$M_{lm} = 2e^{-4} \cdot \cos(\theta) \cdot \left[\begin{aligned} & (u+l) \tanh^{-1} \frac{m}{R_1+R_2} + (v+m) \\ & \cdot \tanh^{-1} \frac{l}{R_1+R_4} - u \cdot \tanh^{-1} \\ & \frac{m}{R_3+R_4} - v \cdot \tanh^{-1} \frac{l}{R_2+R_3} \end{aligned} \right] \quad (1)$$

The filaments with length l and m are at an angle θ and intersect when extended by u and v , with distances R_1 through R_4 between the filament endpoints (Fig. 7). While (1) produces a mutual inductance M_{lm} in nH that is negative for obtuse and positive for acute angles, the sign of M_{lm} depends on the flow of the current and can be determined by the sign of the scalar vector product between the filaments.

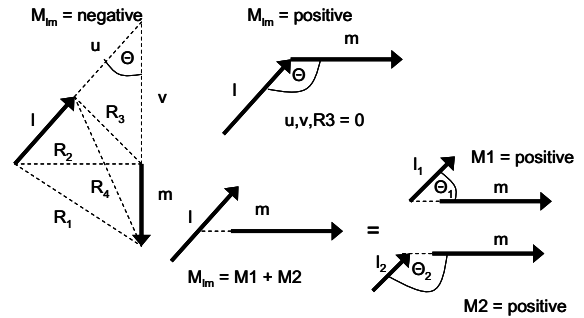


Fig.7. Typical cases for magnetically coupled filaments at an angle.

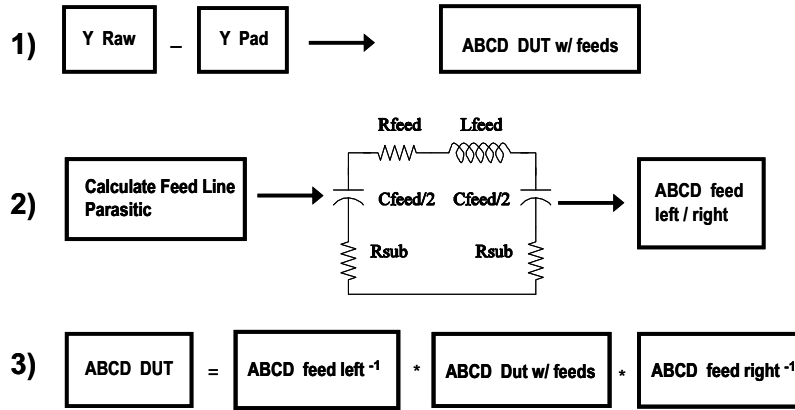


Fig.8. Sequence of 3-step semi-analytical de-embedding process.

The inductance of 2 filaments is the sum of the self-inductances L_l , L_m and twice the mutual M_{lm} :

$$L = L_l + L_m + 2 \cdot \text{sign}(\vec{l} \cdot \vec{m}) \cdot |M_{lm}| \quad (2)$$

B. 3-Step De-embedding Sequence

From layout and electrical specification data an analytical model can be built for the feed-lines. The mutual inductance to the intrinsic device is lumped into the inductance component of the feed-line model. This adjustment will correct for the positive or negative mutual inductance effect exerted by the feed lines. Validity of the de-embedding result over broadband frequencies requires the frequency dependence of resistance, capacitance and substrate parasitic to be included in the lumped model.

RF measurements on THRU line test structures were used to extract and calibrate the feed-line model. The de-embedding technique starts with subtraction of the pad admittance using a simple open test structure with no feed-lines, thus isolating

the feed-line / DUT structure. Next the feed-line models are removed from the DUT data by ABCD matrix multiplication (Fig. 8) yielding the intrinsic device.

Two 1-turn differential inductors with a small inductance value of 290 pH and 390 pH for the half-coils from port to center tab were built in the Jazz Semiconductor 5.3 um thick metal 5 Al SBC18 process and de-embedded using a scalable thru-line [7] and the new semi-analytical approach. While the relatively high Q of ~25 and ~30 is extracted accurately for both de-embedding processes, a clear difference in low frequency inductance of ~13 % is observed, owing to the mutual inductance between feed and DUT (Fig. 9 and Fig.10). In the differential inductor test structure layout (Fig.2), the feed lines exert an overall negative mutual inductance effect, lowering the extracted inductance result obtained with the thru-line or any standard de-embedding process. Consequently, the value of the intrinsic device inductance is underestimated as is shown with the two 1-turn inductors. The frequency dependent Q, L and R results agree well between both approaches. This result underlines that particularly for inductors with high Q and small inductance value, the feed parasitic have to be carefully taken into

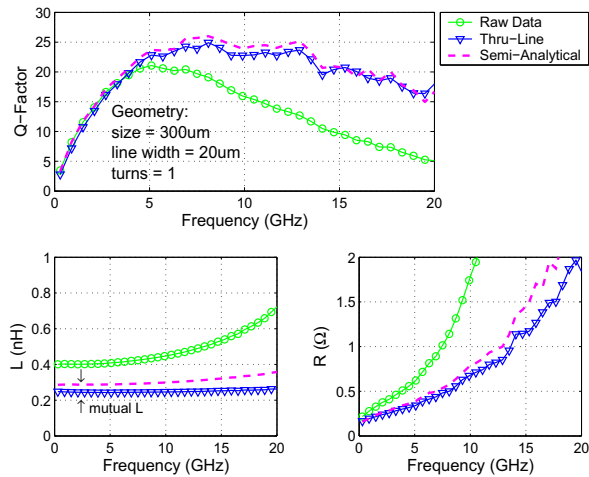


Fig.9. Q, L and R plots for a 1-turn 290 pH differential inductor de-embedded using scalable thru-line and semi-analytical de-embedding..

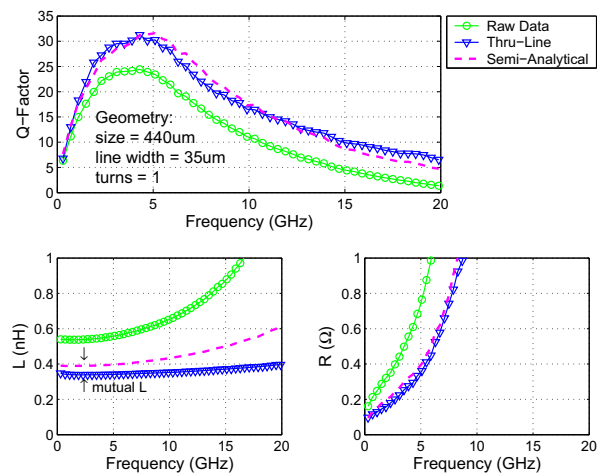


Fig.10. Q, L and R plots for a 1-turn 390 pH differential inductor de-embedded using scalable thru-line and semi-analytical de-embedding..

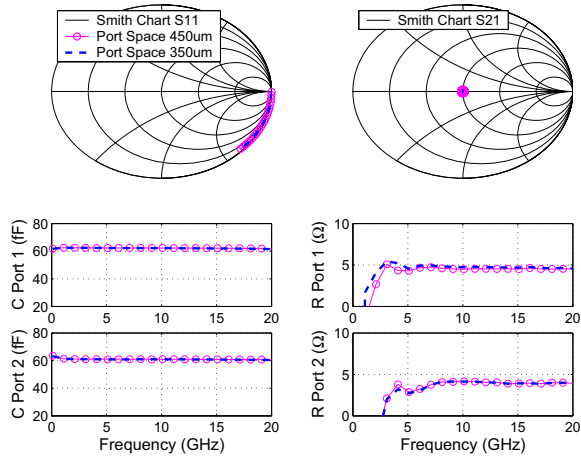


Fig.11. S-parameter and parasitic C, R for pad open structure with 350 μm and 450 μm port spacing.

account if model and measurement accuracy is desired.

This procedure is easily automated by inputting the layout and electrical specification data into a de-embedding macro. In addition, it is very economic in layout space since only one de-embedding structure is necessary, the pad open. Further, it does not require a fixed port to port spacing for the layout of the test structure frame, since the feed-line model is scalable and computed from the specific layout information. This is an important benefit, enabling the RF characterization of a large set of varying inductor sizes with full and partial turn numbers, as are needed to perform model verification for scalable inductor models. Since the pad open structure parasitic is dominated by the capacitance from the signal pad to the metal 1 ground strip underneath (Fig.1,2,3, [8]) and does not vary with the size of the test fixture frame, only one pad open structure is needed to cover various test fixture sizes. The small signal S-parameter and extracted parasitic C, R on a pad open structure with port spacing of 350 μm and 450 μm are virtually identical as is shown with the measurement data in Fig.11.

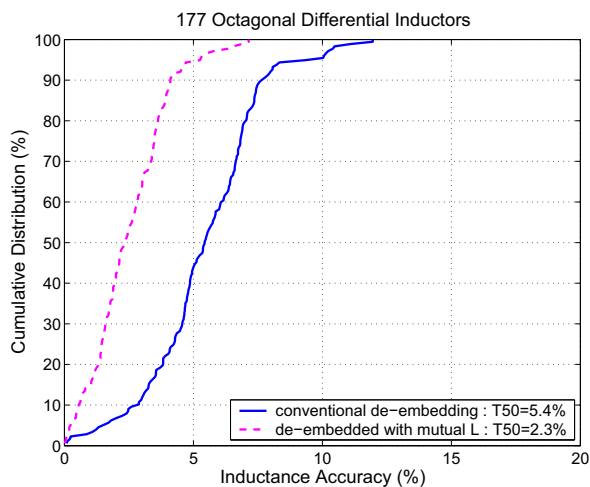


Fig.12. Error of DC inductance for de-embedding with and without taking into account the magnetic coupling to signal feed-lines.

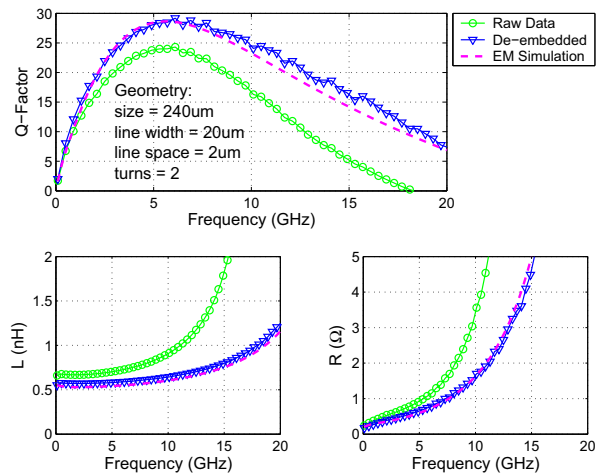


Fig.13. Measured and de-embedded Q, L and R versus Momentum electromagnetic simulation.

IV. MEASUREMENT VALIDATION

A total of 177 octagonal differential inductors from 6 different Jazz backend technologies were measured from 100 MHz to 20 GHz on an Agilent 50 GHz PNA to validate the new de-embedding technique. The measurement setup was de-embedded to the tips of the RF probes using the standard SOLT technique with ceramic calibration substrate [11]. Fig. 12 shows the cumulative error of the dc inductance value of the measured differential inductors for conventional and semi-analytical de-embedding methods, benchmarked against the 3D inductance extraction result from FastHenry [12]. The accuracy of the inductance result improved from a median (T50) of 5.4 % to 2.3 % by accounting for the mutual inductance. It was observed that the error for neglecting the mutual inductance with the feed-lines was larger for square than octagonal inductors due to the longer adjacent length between feed and inductor segments.

The accuracy of the Q, L and R result over broadband frequency was validated also against ADS Momentum

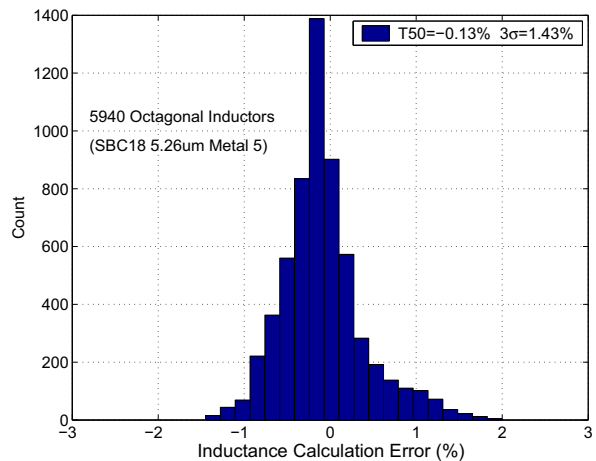


Fig.14. Inductance model accuracy for octagonal inductors.

electromagnetic simulations (Fig.13). The semi-analytical de-embedding method produced accurate results for inductance, resistance, Q and self-resonant frequency and worked well over all inductors measured.

V. CONCLUSIONS

This paper advances the state of the art by presenting for the first time, to the knowledge of the authors, a de-embedding technique which includes the mutual magnetic coupling between an intrinsic inductor DUT and the parasitic feed lines of the test structure. The accuracy of the de-embedded inductance is shown to improve to a median of 2.3%, representing a 57% reduction in the error of previous methods. Inductor models have been previously reported to match within 2 % of the EM simulation result as shown in Fig. 14, [1]. Thus, the new de-embedding methodology reduces the measurement error such that the results are valid for compact model development. The methodology is accurate over various types of inductors, as well as DUT implementation in different RF test structures styles.

REFERENCES

- [1] V. Blaschke and J. Victory, "A Scalable Model Methodology for Octagonal Differential and Single-Ended Inductors," *CICC Proceedings*, Sep.2006.
- [2] M.C.A.M. Koolen, J.A.M Geelen and M.P.J.G. Versleijen, "An Improved De-Embedding Technique for On-Wafer High-Frequency Characterization," IEEE 1991 Bipolar Circuits and Technology Meeting 8.1
- [3] H. Cho and D.E. Burk, "A Three-Step Method for the De-Embedding of High-Frequency S-Parameter Measurements," *IEEE Trans. Electron Devices*, vol. 38, no. 6, Jun. 1991
- [4] T.E. Kolding, "A Four-Step Method for De-Embedding Gigahertz On-Wafer CMOS Measurements," *IEEE Trans. Electron Devices*, vol. 47, no. 4, Apr. 2000
- [5] Q. Liang et al., "A Simple Four-Port Parasitic De-Embedding Methodology for High-Frequency Scattering Parameter and Noise Characterization of SiGe HBTs," *IEEE Trans. MTT*, vol. 51, no. 11, Nov. 2003
- [6] L.F. Tiemeijer, R.J. Havens, A.B.M. Jansman, and Y. Bouttement, "Comparison of the Pad-Open-Short and Open-Short-Load Deembedding Techniques for Accurate On-Wafer RF Characterization of High-Quality Passives," *IEEE Trans. MTT*, vol. 53, no. 2, Feb. 2005
- [7] M.H. Cho, G.W. Huang, K.M. Chen and A.S. Peng, "A Novel Cascade-Based De-Embedding Method for On-Wafer Microwave Characterization and Automatic Measurement," 2004 IEEE MTT-S Digest
- [8] T.E. Kolding, O.K. Jensen, and T. Larsen, "Ground-Shielded Measuring Technique for Accurate On-Wafer Characterization of RF CMOS Devices," IEEE ICMTS, March 2000
- [9] H.M. Greenhouse, "Design of Planar Rectangular Microelectronic Inductors," IEEE Transactions on Parts, Hybrids, and Packaging, Vol. PHP-10, No.2, June 1974.
- [10] F.W. Grover, "Inductance Calculations," Van Nostrand Co. N.Y., 1946, Dover Edition, 2004.
- [11] R.J. Havens, L.F. Tiemeijer, and L. Gambus, "Impact of Probe Configuration and Calibration Techniques on Quality Factor Determination of On-Wafer Inductors for GHz Applications," Proc. IEEE ICMTS, vol.15, Apr. 2002
- [12] FASTHENRY, 3-dimensional inductance extraction program, version 3.0, Department of Electrical Engineering and Computer Science, MIT.